Electronic Supplementary Information : Prediction of structural and thermomechanical properties of polymers from multiscale simulations

Gaëtan Maurel [a,b], **Florent Goujon**[a], **Benoit Schnell** [b], **Patrice Malfreyt**[*a]

1 Relaxation of the polymer chains: Atomistic versus coarse-grained descriptions

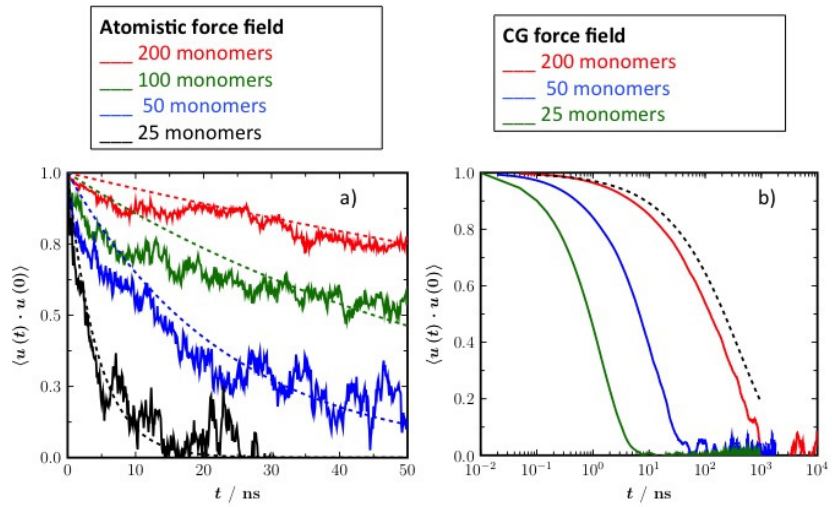

Fig. S 1 End-to-end vector autocorrelation functions calculated for different polymer chain lengths by using a) the atomistic and b) the mesoscopic simulations. The fitting curves in part a) (dotted lines) result from the Kolrausch-Williams-Watts stretched exponential form. The dotted line in part b) represents the fitting curve of the autocorelation function calculated from atomistic models for a polymer chain length of 200 monomers.

The dynamical properties of the *cis*-1,4-PB bulk are illustrated in Fig. S1 through the end-to-end vector autocorrelation function calculated with different polymer chain lengths ranging from 25 to 200 monomers. Parts a) and b) of Fig.S1 represent the autocorrelation functions calculated from atomistic and mesoscopic simulations, respectively. For the atomistic models, the function $< \mathbf{u}(t) \cdot \mathbf{u}(0) >$ where $\mathbf{u}$ is the unit vector directed along the chain end-to-end vector does decay to zero only for a polymer chain length of 25 monomers. However, this chain length of 25 monomers corresponds rather to that of an oligomer and cannot be used to simulate entangled polymer chains. From a polymer chain length of 50 monomers, the function does not decay to zero by the end of the 50 ns indicating an insufficient relaxation of the polymer chains. We also plot for comparison the curves resulting from the Kolrausch-Williams-Watts $G(t) = (\exp(-t/\tau)^{\beta})$. where $\beta < 1$ suggests the presence of entanglements. The calculated values of the average relaxation time $< \tau_c >= \int_0^{\infty} G(t)dt = \frac{\tau}{\beta}\Gamma(1/\beta)$ ranges from 4.4 to 530 ns when the polymer chain length increases from 25 to 200 monomers. We conclude that the atomistic model is unable to simulate a well-equilibrated polymer melts of entangled chains with a reasonable computational time. Part b) of Fig.S1 shows that the autocor-

relation functions calculated by using the CG models are able to decay to zero within the simulation time for the different polymer chain lengths. For the longest polymer chain length of 200 monomers, the DPD simulations show a function that decays to zero at a value slightly larger than 1 μs. A typical simulation over 2 μs would require 1000 days for there atomistic models against 10 days for the CG models over a parallel architecture of 12 processors. These curves conclude on the inability of the atomic description to model entangled polymers over large time scales with a reasonable computational cost.

2 Atomistic simulations

The atomistic simulation of polymer melts of relatively long chains requires to check some structural and thermodynamic properties that can be impacted by an insufficient equilibration of the polymer chains. As a consequence, we have to check that the calculated properties have well-converged during the acquisition period. Part a) of Fig.S2 shows the distributions of the end-to-end distances of the chains in a melt of *cis*-1,4-PB. First, the distributions calculated in the equilibration and production periods differ significantly. In addition, the production phase has provided a gaussian distribution of the end-to-end distance with an average value of 0.74 Å^2 g mol^{-1} against an experimental value of 0.76 Å^2 g mol^{-1}. The ratio to the mean square end-to-end distance to the mean square radius of gyration is then equal to 6.1 in line with the expected value of 6 for ideal gaussian chains[1].

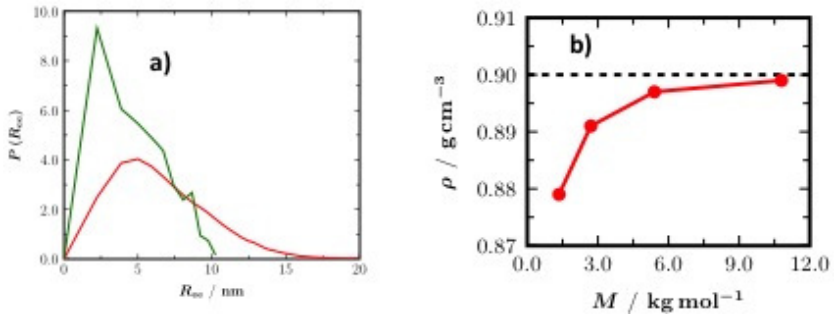

Fig. S 2 a) Distribution of the end-to-end distances calculated in a melt of *cis*-1,4-PB chains of 200 monomers during the equilibration and acquisition phases. b) Polymer melt density calculated at 300 K for different molar masses. The dotted line in b) corresponds to the experimental values[2].

We report the polymer melt density as a function of the polymer chain length in part b) of Fig.S2. We establish a clear dependence of the chain length on the melt density. We also show that the reproduction of the polymer melt density is possible with the value of the molar mass used in this paper. We can conclude, that the methodology used here (force field, box sizes, lengths of the equilibration and production phases, polymer molecular weight, number of polymer chains) is able to reproduce the main static features of the polymer melt.

3 Performance of the CG force field

3.1 Equilibration of polymer melts of entangled polymer chains

We focus here on the ability of the CG simulations to give well-relaxed polymer melts within a reasonable computational effort. Fig. S3 represents the quantity R_{ij}^2/n_{ij} of *cis*-1,4-PB polymer chains as a function of the number of bonds in a subchain. R_{ij} is the mean distance of the subchain formed by n_{ij} bonds. The asymptotic value of 2.05 nm^2 is calculated from the quantity $M_o R_{ee}^2/M$ and the experimental value R_{ee}^2/M = 0.758 Å^2 mol g^{-1} where M_o is the molar mass of a bead (270 g mol^{-1}) and R_{ee} the end-to-end distance[2]. This limit value is represented in Fig. S3 by a dotted line. We also reports the same property calculated using atomistic models. The atomistic simulations were performed from 40 chains of 800 united atoms per chains corresponding to a polymer chain length of 200 monomers. The CG simulations were carried out with 20 chains of 160 beads corresponding to 20 chains of 800 monomers. The x-axis is labelled using the number of both united atoms and beads. First, we observe that the atomistic simulations allow to reach just the plateau in spite of the computational effort required to model such a system-size. Second, the DPD simulations reproduce very well the asymptotic behavior and the expected experimental value[2] is reached from a polymer chain length of 50 beads. The CG modelling of a long polymer chain of 160 beads indicates that the polymer melt is fully equilibrated with a computational CPU time roughly reduced by a factor of 20 with respect to atomistic chains 4 times smaller.

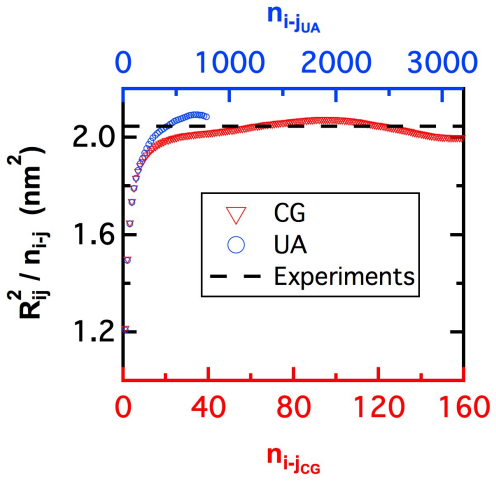

Fig. S 3 R_{ij}^2/n_{ij} ratio as a function of the number of beads (bottom axis) and united atoms (top axis) calculated for the *cis*-1,4-PB polymer chains. The dotted line corresponds to the experimental value[2].

3.2 Transferability of the CG force field

We illustre the ability of the CG force field to be transferable to different different polymer chain lengths by reporting in Table S1 the simulated melt density and end-to-end distances of different polymers. The

CG models are developed from a polymer chain length to 200 monomers. The transferability in the polymer chain length is then investigated by applying these potentials for larger polymer chain lengths of 800 monomers. For the same degree of coarse-graining, we observe that increasing the polymer chain length does not affect the quality of the reproduction of the melt density and the end-to-end distance. It shows a certain transferability of the CG models. It opens the way of using these CG models for polymer chain lengths larger than those used for their development.

Table S 1 Polymer melt density(ρ), end-to-end distance (R_{ee}/M), ratio to the mean square end-to-end distance to the mean square radius of gyration, The experimental values for each polymer are taken from Ref. 2. The subscripts give the accuracy of the last decimal(s), i.e., 0.900_9 means 0.900 ± 0.009.

	ρ (g cm^{-3})		R_{ee}/M (Å^2 mol g^{-1})		R_{ee}^2/R_G^2
	CG	Exp.	CG	Exp.	
		$\lambda = 4$			
cis-1,4-PB	0.900_9	0.900	0.74_7	0.76	6.3
		$\lambda = 5$			
cis-1,4-PB	0.885_1	0.900	0.71_8	0.76	5.9
		$\lambda = 5$, N = 40 beads = 200 monomers			
cis-1,4-PB	0.885_1	0.900	0.71_8	0.76	5.9
PIB	0.920_1	0.918	0.52_6	0.57	6.2
PDMS	0.968_7	0.970	0.42_4	0.42	6.1
		$\lambda = 5$, N = 160 beads = 800 monomers			
cis-1,4-PB	0.907_1	0.900	0.78_8	0.76	6.1
PIB	0.925_1	0.918	0.61_5	0.57	6.2
PDMS	0.973_5	0.970	0.42_3	0.42	6.3

3.3 Impact of the degree of coarse-graining

The impact of corse-graining is studied by developing new potentials by using a degree of coarse-graining $\lambda = 4$. The simulated density and end-to-end distances are then listed in Table S1. We observe that the performance of the reproduction remains identical to that obtained with $\lambda = 5$. In addition, Fig.S4 shows that the fluctuations in the density are weaker with $\lambda = 4$ than with $\lambda = 5$. This underlines the role of the degree of coarse-graining on the compressibility of the system. This represents a possible factor that may contribute to the significant deviations (two orders of magnitude) of the isothermal compressibility from the corresponding experimental value.

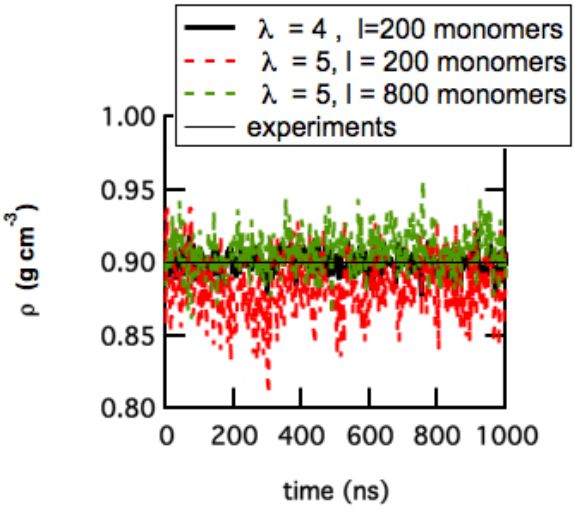

Fig. S 4 Simulated polymer density as a function of time for two different degrees of coarse-graining and two different polymer chain lengths of 200 and 800 monomers.

4 Application of an uniaxial deformation

First, Fig. S5a shows the trajectory of the L_z dimension at different stress constraints. We observe that a period of 900 ns is required to obtain the convergence of L_z. We also check that the effect of the stress constraint is clearly observable on the trajectory of L_z demonstrating the ability of the DPD simulations for evaluating ε_z. Fig. S5b establishes a Poisson's ratio ν of 0.5 ensuring the volume constant during the deformation as assumed in the affine model[3].

By using the theory of the affine network[3,4], the elastic free energy of deformation is given by

$$\begin{aligned}\Delta A^{\text{affine}} &= \frac{N_p}{2}k_BT(\lambda_x^2+\lambda_y^2+\lambda_z^2-3)\\ &\quad -N_jk_BT\ln(\lambda_x\lambda_y\lambda_z) \qquad (1)\\ &= \frac{N_p}{2}k_BT(\lambda^2+2(V/V_o)\lambda^{-1}-3)\\ &\quad -N_jk_BT\ln(V/V_0) \qquad (2)\end{aligned}$$

where $\lambda_x=\lambda_y=(\frac{V}{V_o\lambda})^{1/2}$ and $\lambda_z=\lambda=L_z/L_{z,0}$. V_0 is the initial volume and $L_{z,0}$ is the box length in the z-direction. N_p and N_j are the number of polymer chains and junctions in the network. In this model it was assumed that the local deformations are the same as the macroscopically imposed deformation. The force

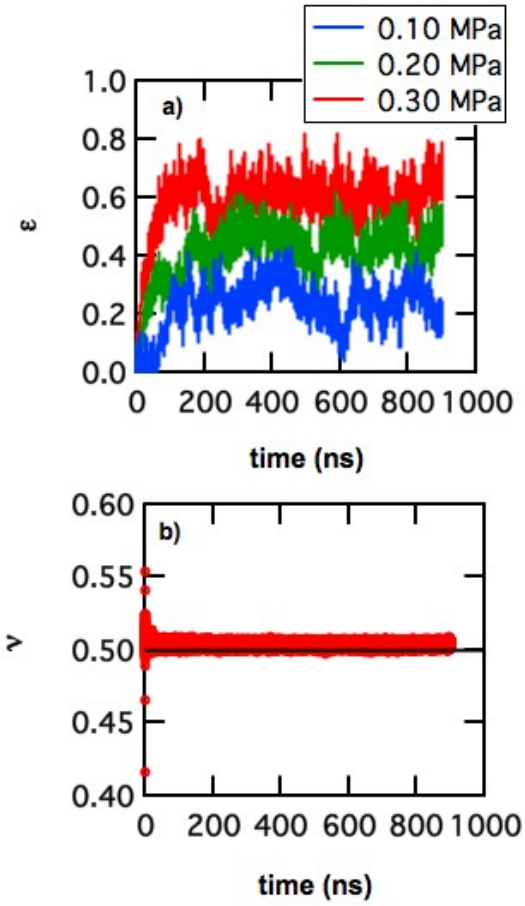

Fig. S 5 a) Trajectories of the elongations of the box length along the z-dimension for three stress values indicated in the legend and b) trajectory of the Poisson's ratio calculated for an uniaxial weak elongation.

f^{affine} under uniaxial tension along z is defined as

$$f^{\text{affine}} = \left(\frac{\partial \Delta A_{\text{affine}}}{\partial L}\right)_{T,V} = \frac{1}{L_{z,0}}\left(\frac{\partial \Delta A_{\text{affine}}}{\partial \lambda}\right)_{T,V} \tag{3}$$

$$= \frac{1}{L_{z,0}} N_p k_B T \left(\lambda - \lambda^{-2}\right) \tag{4}$$

The stress calculated in the tensile z-direction is then given by

$$\sigma_{zz}^{\text{affine}} = \frac{f^{\text{affine}}}{A_0} = \frac{\rho RT}{M_c}\left(\lambda - \lambda^{-2}\right) \tag{5}$$

where $A_0 = L_{x,0}L_{y,0}$. M_c and ρ are the molecular weight of the polymer chains between the junctions and density, respectively.

In the phantom model[5,6], the elastic free energy is then given by

$$\begin{aligned}\Delta A^{\text{phantom}} &= \frac{N_p}{2}\left(1-\frac{2}{\phi}\right)k_BT(\lambda_x^2+\lambda_y^2+\lambda_z^2-3) \\ &\quad -N_jk_BT\ln(\lambda_x\lambda_y\lambda_z) \qquad (6)\\ &= \frac{N_p}{4}k_BT(\lambda^2+2(V/V_o)\lambda^{-1}-3) \\ &\quad -N_jk_BT\ln(V/V_0) \qquad (7)\end{aligned}$$

where ϕ represents the crosslink functionality. Here we model a tetrafunctionnal network ($\phi = 4$).

$$f^{\text{phantom}} = \left(\frac{\partial \Delta A^{\text{phantom}}}{\partial L}\right)_{T,V} = \frac{1}{2L_{z,0}}N_pk_BT\left(\lambda-\lambda^{-2}\right) \qquad (8)$$

The stress calculated in the phantom model is described by the following expression

$$\sigma_{zz}^{\text{phantom}} = \frac{f^{\text{phantom}}}{A_0} = \frac{\rho RT}{2M_c}\left(\lambda-\lambda^{-2}\right) \qquad (9)$$

In the elastic region, at weak elongations, the Young's modulus E is defined as the ratio of the longitudinal stress σ_{zz} to the longitudinal strain ε_z according to

$$\sigma_{zz} = E\varepsilon \qquad (10)$$

By replacing λ by $\varepsilon+1$ into Eqs.(5) and (9), we obtain

$$\sigma_{zz}^{\text{affine}} = \frac{f^{\text{affine}}}{A_0} = \frac{\rho RT}{M_c}\left(1+\varepsilon-(1+\varepsilon)^{-2}\right) \qquad (11)$$

$$\sigma_{zz}^{\text{phantom}} = \frac{f^{\text{phantom}}}{A_0} = \frac{\rho RT}{2M_c}\left(1+\varepsilon-(1+\varepsilon)^{-2}\right) \qquad (12)$$

In the case of weak deformations ($\varepsilon_z \to 0$), the stress expresses as

$$\sigma_{zz}^{\text{affine}} = \frac{f^{\text{affine}}}{A_0} = \frac{\rho RT}{M_c}\left(3\varepsilon\right) \qquad (13)$$

$$\sigma_{zz}^{\text{phantom}} = \frac{f^{\text{phantom}}}{A_0} = \frac{\rho RT}{2M_c}\left(3\varepsilon\right) \qquad (14)$$

In the elastic region of the deformations, the Young's modulus can be related to the shear modulus G by

$$G = \frac{E}{2(1+\nu)} = \frac{E}{3} \quad \text{with } \nu = 0.5 \qquad (15)$$

leading to

$$G^{\text{affine}} = \frac{\rho RT}{M_c} \tag{16}$$

$$G^{\text{phantom}} = \frac{\rho RT}{2M_c} \tag{17}$$

From the linear regime (shown in the inset of Fig. S6), we extract a Young's modulus $E = \frac{\partial \sigma_{zz}}{\partial \varepsilon} = 0.57$ MPa. The slope, shown by the dotted line in Fig. S6, matches very well the $\sigma_{zz}^{\text{phantom}} = f(\varepsilon)$ curve at weak elongations establishing the linearity of our deformations. From this curve, we calculate $G = E/3 = 0.19$ MPa.

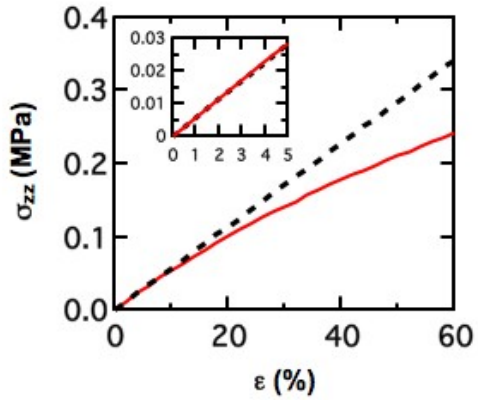

Fig. S 6 Stress-strain curve of uniaxial deformation as a function of ε. The inset focuses on the region of weak deformations to show the linear behavior (black dotted line) of the fitting curve (red curve).

References

1 M. Rubinstein and R. H. Colby, *Polymer Physics*, Oxford University Press, Oxford, 2003.
2 L. J. Fetters, D. J. Lohse, D. Richter, T. A. Witten and A. Zirkel, *Macromolecules*, 1994, **27**, 4639–4647.
3 L. R. G. Treolar, *The Physics of Rubber Elasticity*, Clarendon Press, Oxford, 1975.
4 W. Kuhn, *J. Polym. Sci. Part A: Polym. Phys.*, 1946, **1**, 380–388.
5 H. M. James, *J. Chem. Phys.*, 1947, **15**, 651–668.
6 H. M. James and E. Guth, *J. Chem. Phys.*, 1947, **15**, 669–684.